LETTER

doi:10.1038/nature10118

XUTs are a class of Xrn1-sensitive antisense regulatory non-coding RNA in yeast

E. L. van Dijk[1]*, C. L. Chen[1]*, Y. d'Aubenton-Carafa[1], S. Gourvennec[2], M. Kwapisz[2], V. Roche[2], C. Bertrand[2], M. Silvain[1], P. Legoix-Né[3], S. Loeillet[4], A. Nicolas[4], C. Thermes[1] & A. Morillon[1,2]

Non-coding (nc)RNAs are key players in numerous biological processes such as gene regulation, chromatin domain formation and genome stability[1,2]. Large ncRNAs interact with histone modifiers[3–5] and are involved in cancer development[6], X-chromosome inactivation[7] and autosomal gene imprinting[8]. However, despite recent evidence showing that pervasive transcription is more widespread than previously thought[9], only a few examples mediating gene regulation in eukaryotes have been described[10]. In *Saccharomyces cerevisiae*, the bona-fide regulatory ncRNAs are destabilized by the Xrn1 5′–3′ RNA exonuclease[11,12] (also known as Kem1), but the genome-wide characterization of the entire regulatory ncRNA family remains elusive. Here, using strand-specific RNA sequencing (RNA-seq), we identify a novel class of 1,658 Xrn1-sensitive unstable transcripts (XUTs) in which 66% are antisense to open reading frames. These transcripts are polyadenylated and RNA polymerase II (RNAPII)-dependent. The majority of XUTs strongly accumulate in lithium-containing media, indicating that they might have a role in adaptive responses to changes in growth conditions. Notably, RNAPII chromatin immunoprecipitation followed by DNA sequencing (ChIP-seq) analysis of Xrn1-deficient strains revealed a significant decrease of RNAPII occupancy over 273 genes with antisense XUTs. These genes show an unusual bias for H3K4me3 marks and require the Set1 histone H3 lysine 4 methyl-transferase for silencing. Furthermore, abolishing H3K4me3 triggers the silencing of other genes with antisense XUTs, supporting a model in which H3K4me3 antagonizes antisense ncRNA repressive activity. Our results demonstrate that antisense ncRNA-mediated regulation is a general regulatory pathway for gene expression in *S. cerevisiae*.

Antisense ncRNAs in yeast control Ty1 mobility[12,13] and *PHO84* transcription through histone modifications[11,12] in an RNA-interference-independent manner[14] (Supplementary Fig. 1). The regulatory ncRNAs are distinct from the canonical cryptic unstable transcripts (CUTs) of shorter size, destabilized by the nuclear exosome[15]. In contrast, the regulatory antisense ncRNAs are mainly degraded by the cytoplasmic 5′–3′ Xrn1 exonuclease[16]. These features suggest that yeast antisense regulatory ncRNAs belong to a separate class of unstable transcripts. Here, we address their systematic identification by characterizing the Xrn1-dependent cryptic transcriptome.

We analysed the whole transcriptome in wild-type and *xrn1Δ* strains (Fig. 1a). Because Xrn1 mainly acts downstream of RNA deadenylation[16], we analysed total RNA depleted for ribosomal RNAs (ribo$^-$) and subsequently compared with fractions enriched for polyadenylated RNAs (polyA$^+$) (Supplementary Fig. 2). Ultra-deep sequencing produced 84 and 134 millions of unique reads for ribo$^-$ preparations from wild-type and *xrn1Δ* strains, respectively (Supplementary Table 1), reaching unprecedented coverage of the yeast cryptic transcriptome[17–19]. Read densities were normalized with transfer RNAs and small nucleolar RNAs insensitive to Xrn1 activity[20,21] (Methods and Supplementary Fig. 3). Similar results were obtained with biological duplicates and with ABI-SOLiD or Illumina sequencing technologies (Supplementary Fig. 4a, b). Transcripts were identified along read density profiles and compared to annotated open reading frames (ORFs) and stable uncharacterized transcripts (SUTs)[22] (Methods and Supplementary Fig. 5). The Xrn1-deficient strain showed an average 4.4- to 3.9-fold increase of ORF and dubious ORF transcripts, respectively (Fig. 1b and Supplementary Fig. 6a, b), further establishing Xrn1 as the major exonuclease responsible for messenger RNA turnover[16]. The data revealed 932 previously uncharacterized ncRNAs (New) presenting a 10.8-fold average increase in the *xrn1Δ* strain (Fig. 1b, c and Supplementary Fig. 6c). Additionally, 75% (543) of the SUTs described in rich media[22] showed an unexpected 9.6-fold increase in the *xrn1Δ* strain, indicating that Xrn1 is also active on these ncRNAs (Fig. 1c and Supplementary Fig. 6d). In contrast to the majority of CUTs, 20% (183) of them were highly sensitive to Xrn1 (7.9-fold increase, Fig. 1c and Supplementary Fig. 6e), showing that a subclass of CUTs escapes from exosome-dependent nuclear degradation, as previously suggested[23]. Thus, we describe 1,658 ncRNAs that are Xrn1-sensitive unstable transcripts (XUTs), of which 66% are antisense to ORFs (Fig. 1b, c). The start sites of three XUTs upstream of the *SUC2* locus (*SUC2uxut*) (Fig. 1d) were identified by 5′ rapid amplification of cDNA ends (5′RACE) experiments (Supplementary Fig. 7). Northern blot analyses (Fig. 1e) showed that the levels of *SUC2uxut1* and *SUC2uxut3* are independent of Trf4, subunit of the TRAMP complex, required for CUT degradation[24]. This confirms that XUTs encompass a distinct class of cryptic transcripts. Further analyses showed that XUTs are polyadenylated and synthesized by RNAPII (Methods and Supplementary Fig. 8a–d).

We asked whether changes in growth conditions would activate XUTs in wild-type cells. Interestingly, lithium toxicity is due to inactivation of Xrn1, Rat1 and RNase MRP[25] and might be associated with XUT overexpression. The kinetics of appearance of selected XUTs in lithium-containing media (Fig. 2a and Supplementary Fig. 9) showed that the Ty1-ncRNA (*RTL*) appears before 30 min, similarly to *SUC2uxut1* and *TPO1axut* (transcriptome details in Supplementary Fig. 10a). After washing and further growth, cells present a dramatic decrease of XUTs levels, indicating a highly dynamic XUT accumulation. RNA-seq analyses after 80 min in lithium media showed XUTs overexpression (Fig. 2b) and 56% of them have similar RNA levels as the *xrn1Δ* strain (Fig. 2c). To note, some XUTs present a milder sensitivity to lithium as exemplified by *SUC2uxut2* and *SUC2uxut3* (Fig. 2a, d). These results indicate that a majority of XUTs rapidly and reversibly accumulate after lithium addition, indicating a role in the early response to this growth media change.

We tested whether antisense ncRNA accumulation controls sense gene transcription as for Ty1 (ref. 12). ChIP-seq analyses identified 996 ORFs with reduced RNAPII occupancy in the *xrn1Δ* strain (Fig. 3a, $P < 0.01$, Methods); among them, 273 (27%) accumulate antisense

[1]Centre de Génétique Moléculaire (CNRS UPR 3404), avenue de la Terrasse, 91198 Gif sur Yvette, France. [2]ncRNA, epigenetic and genome fluidity, Institut Curie, Centre de recherche, CNRS UMR3244, Université Pierre et Marie Curie, 26 rue d'Ulm, 75248 Paris Cedex 05, France. [3]NGS Platform, Institut Curie, 26 rue d'Ulm, 75248 Paris Cedex 05, France. [4]Recombination and Genome instability, Institut Curie, Centre de recherche, CNRS UMR3244, Université Pierre et Marie Curie, 26 rue d'Ulm, 75248 Paris Cedex 05, France.
*These authors contributed equally to this work.

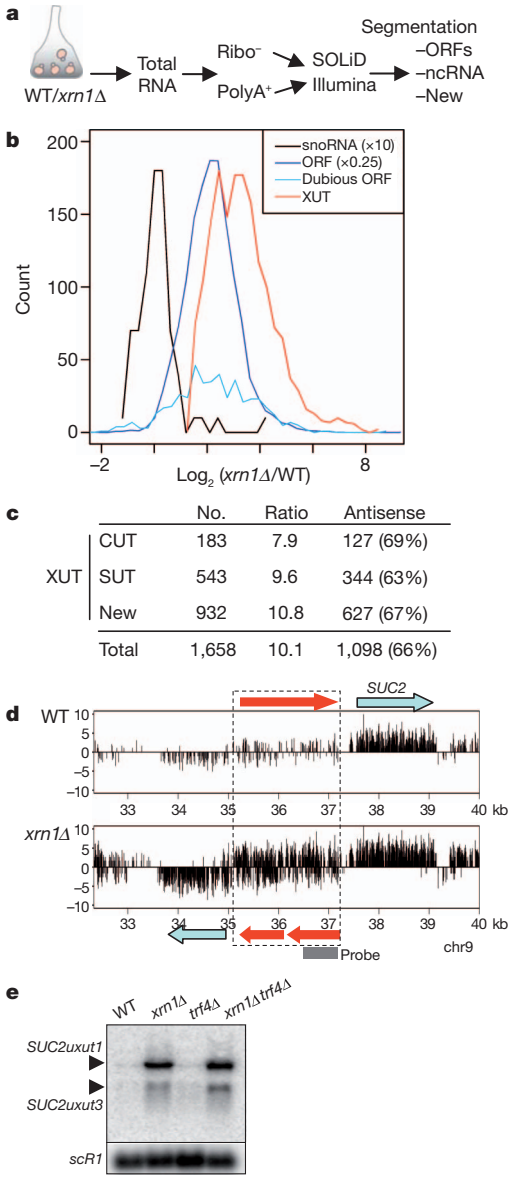

Figure 1 | Cytoplasmic 5′–3′ RNA decay controls a class of cryptic ncRNA. **a**, RNA-seq analyses using wild-type (WT) and *xrn1Δ* strains. Cells were grown in rich media and cDNA sequenced with SOLiD or Illumina technologies (Methods). Segmentation defines transcriptional units (ORFs, ncRNAs, unidentified transcripts (New)). **b**, XUTs define a novel class of ncRNAs. Tag density ratio distributions of *xrn1Δ*/WT for snoRNAs, ORFs and XUTs. **c**, Numbers of XUTs including new ncRNAs (New), most SUTs and few CUTs; average ratios of *xrn1Δ*/WT, numbers and percentage of XUTs antisense to ORFs. **d**, Transcriptome data for *SUC2* locus. Three XUTs (red) were identified within *SUC2* promoter in both orientations; bars, $\log_2$ read numbers (upward and downward, Watson and Crick strands, respectively); grey bar, probe used in **e**. **e**, Northern blot for indicated strains of sense *SUC2uxut1* (2.3 kb) and antisense *SUC2uxut3* (1 kb), using a double-stranded probe (**d**) and control *scR1*.

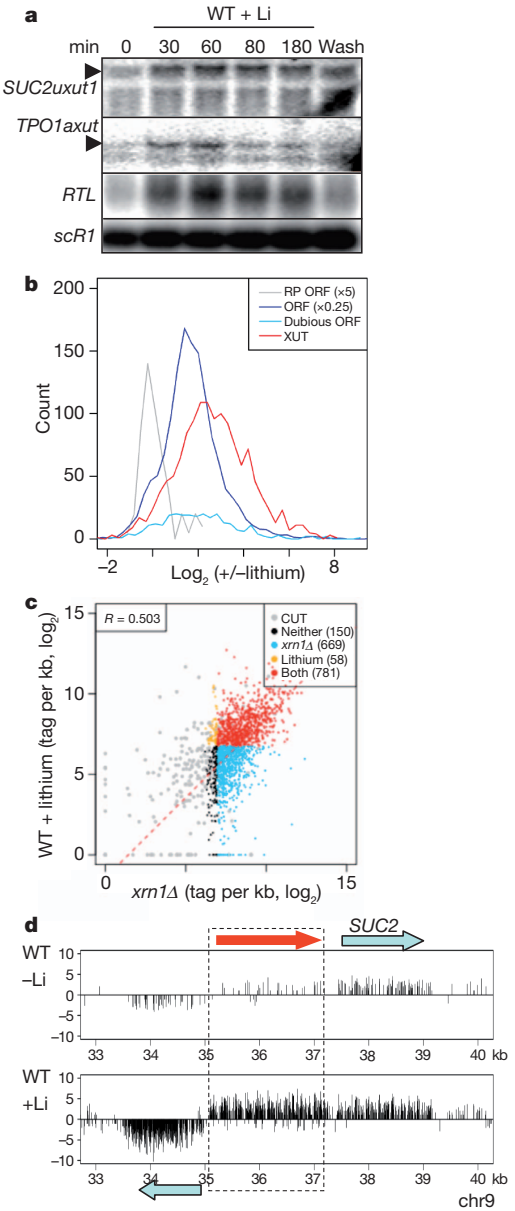

Figure 2 | XUT ncRNAs accumulate in wild-type cells grown in presence of lithium. **a**, XUT levels rapidly increase upon lithium treatment. Northern blot of total RNA from wild-type cells grown without and with 100 mM lithium at different times (Methods); strand-specific probes for *SUC2uxut1* and *SUC2uxut3* as in Fig. 1e, *TPO1axut* and *TY1* XUTs (*RTL*). **b**, XUTs are overexpressed in lithium media. Same as in Fig. 1b with wild type with or without lithium. Ribosomal protein genes were used as reference (grey, Methods). **c**, Tag density of XUTs and CUTs in *xrn1Δ* (abscissa) and WT + lithium (ordinate); 56% of XUTs are similarly expressed in *xrn1Δ* and WT grown in lithium (80 min). XUT expression compared to CUT expression (grey). In the subset of XUTs expressed at higher level than 75% of CUTs, 669 are found in *xrn1Δ* only (blue), 58 in lithium only (yellow) and 781 in both conditions (red). **d**, Same as in Fig. 1d with wild-type cells with or without lithium.

XUTs (Fig. 3a, class 1, Supplementary Table 2). This proportion is larger than for the ORFs that do not present significantly reduced RNAPII levels ($P < 10^{-15}$, chi-squared test; only 15% associate with antisense XUTs), indicating that sense transcriptional silencing correlates with antisense RNA accumulation. Although RNA stabilization in *xrn1Δ* strain could mask potential transcriptional repression, we identified 72 downregulated genes with antisense XUTs (Supplementary Fig. 12) among which 65 showed reduced RNAPII occupancy (Supplementary Fig. 13 and Supplementary Table 3). We conclude that, even though RNA-seq is more suitable to characterize XUT transcripts, ChIP-seq analyses identify extensively downregulated genes like *TIR1* and *TPO1* (Fig. 3b and Supplementary Fig. 10c, transcriptomes in Fig. 4b and Supplementary Fig. 10a). In these cases, RNAPII is almost undetectable within the XUTs' loci in the *xrn1Δ* strain, indicating that either antisense transcription is also silenced or XUT transcription is too low for detection. To establish that XUT accumulation and gene silencing are direct consequences of *XRN1* deletion, we performed *xrn1* conditional inactivation (*xrn1ts*[26], Methods). Not only do 70% of XUTs share identical expression in *xrn1Δ* and *xrn1ts* strains (Supplementary Fig. 14), but both strains also show similar RNAPII occupancies on a selection of class 1 genes (Figure 3c). This suggests

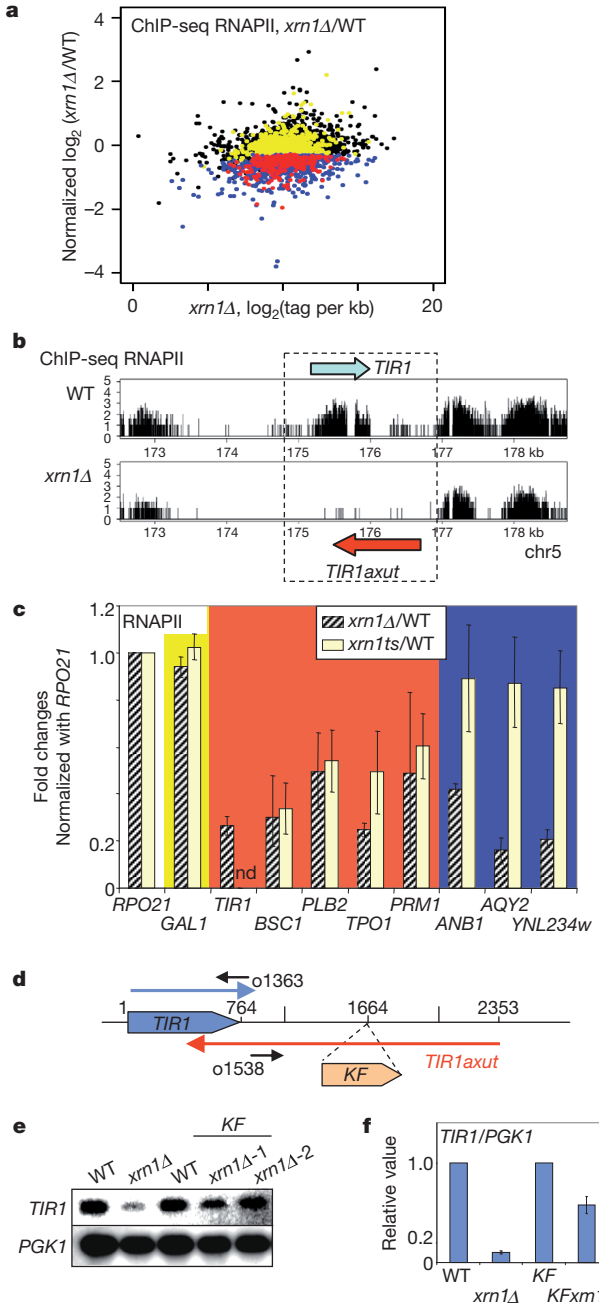

Figure 3 | Transcriptional gene silencing correlates with antisense XUT accumulation. **a**, ORFs with reduced tag densities in *xrn1Δ* strain compared to wild type by RNAPII ChIP-seq analysis ($P < 0.01$, Methods). Selected reduced ORFs associated with (class 1, red) or without antisense XUT (class 2, blue); ORFs with no significant variation with antisense XUT ($P > 0.01$, class 3, yellow) or without (class 4, black). **b**, ChIP-seq density profiles of *TIR1* locus in wild-type and *xrn1Δ* strains. **c**, RNAPII-ChIP analyses by quantitative PCR (mean ± s.d., $n = 3$) using primers within class 4: *RPO21*; class 3: *GAL1*; class 1: *TIR1*, *TPO1*, *BSC1*, *PLB2*, *PRM1* and class 2: *ANB1*, *AYQ2*, *YNL234w*, using wild-type, *xrn1Δ* and *xrn1ts* strains. *xrn1Δ*/*WT* and *xrn1ts*(37 °C)/WT(37 °C) RNAPII ratios normalized by *RPO21*. *xrn1ts* ChIP was performed after 180 min at 37 °C. *TIR1* expression was undetectable upon heat shock (nd). Colours as in **a**. **d**, *TIR1* locus and insertion of the *KANMX* cassette. Probes to detect sense and antisense RNAs are indicated. **e**, *TIR1* RNA levels are directly controlled by *TIR1axut*. Northern-blot with polyA$^+$ RNA using sense-specific probes to detect *TIR1* and *PGK1* mRNAs. Strains: WT, *xrn1Δ*, *KFWT* and *KFxrn1Δ* (two clones). **f**, Quantification of three independent Northern blots using *PGK1* for normalization (mean ± s.d., $n = 3$); respective wild-types were set to 1.

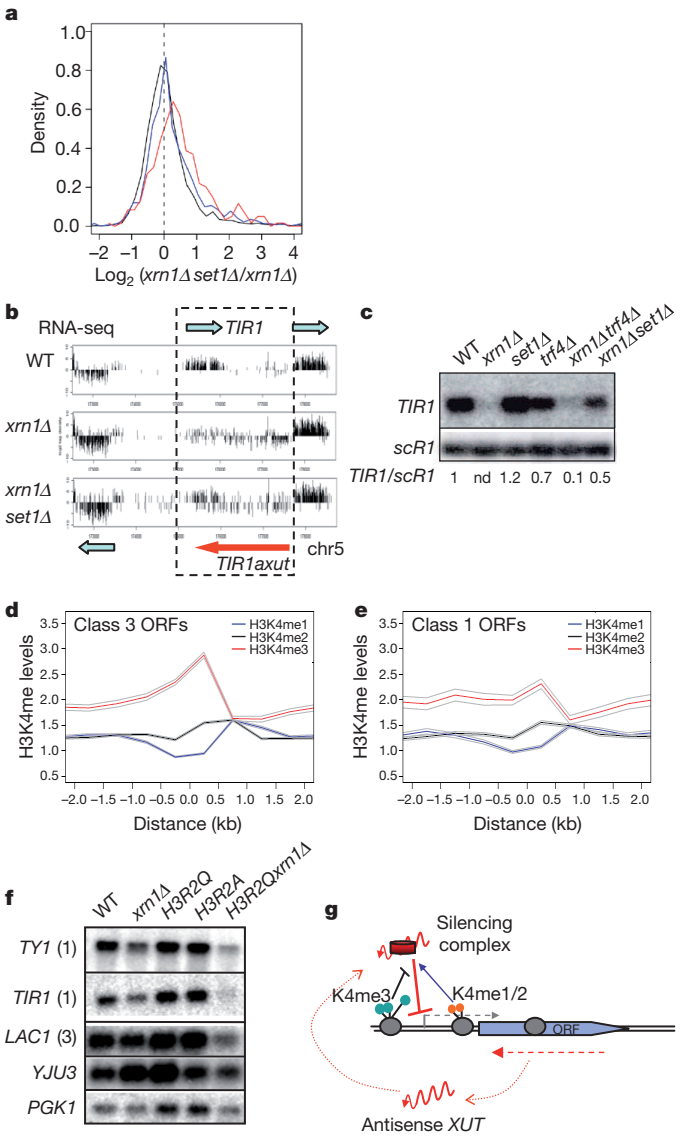

Figure 4 | Antisense XUTs mediate transcriptional gene silencing through Set1-dependent histone methylation. **a**, Repression of class 1 genes partly depends on Set1. Distributions of the $\log_2$ ratios of RNA-seq tag densities *xrn1set1Δ*/*xrn1Δ* for the ORFs; class 1, red; class 2, blue; others, black. **b**, *TIR1* locus transcriptomes in WT, *xrn1Δ* and *xrn1Δset1Δ* strains. Blue arrow, *TIR1* RNA; red arrow, *TIR1axut*; settings as in Fig. 1d. **c**, Northern blot validation of **b** with total RNAs. from indicated strains; probes as in Fig. 3f. **d, e**, Histone H3K4 methylation (mean ± s.e.m.) for genes with antisense XUTs in class 3 ($n = 820$) and class 1 ($n = 273$), respectively. Data from wild type retrieved from previous publication[28] were plotted for H3K4me1 (blue), H3K4me2 (black) and H3K4me3 (red); abscissa, distance to start codon (kb). **f**, Northern blot of polyA$^+$ RNA revealing genes with antisense XUTs: *TIR1*, *TY1* (class 1), *LAC1* (class 3), or without: *YJU3*, *PGK1* (class 4) for indicated strains. Note that *TIR1* and *TY1* mRNAs are less sensitive to *xrn1Δ* due to background differences. **g**, Model depicting XUT-mediated repressive transcriptional activity enhanced by H3K4me1/2 (orange) and antagonized by H3K4me3 (blue).

that class 1 genes are controlled by Xrn1, potentially through their respective antisense ncRNAs. Interruption of the *TIR1axut* in the *xrn1Δ* strain (Fig. 3d and Supplementary Fig. 15) re-established 70% of the *TIR1* mRNA level (Fig. 3e, f). Residual *TIR1axut* detection, due to either alternative initiation start sites of antisense ncRNAs or read-through over the inserted cassette, might explain the residual repressive activity on *TIR1*. Altogether, these data strongly support a direct role for antisense XUTs in gene silencing.

The ncRNA-mediated *TY1* silencing requires the Set1 activity[12] which represses basal transcription of many genes associated with antisense

transcripts[27]. RNA-seq analyses performed in a *set1Δxrn1Δ* strain revealed that only the class 1 genes have higher RNA levels in the absence of Set1 (Fig. 4a; $P < 10^{-6}$, one-tailed two-sample Kolmogorov–Smirnov test), indicating that Set1 has a widespread role in antisense ncRNA-mediated gene repression. Remarkably, Set1 is not involved in XUT expression because the *set1Δxrn1Δ* and *xrn1Δ* strains showed similar levels of XUTs (Supplementary Fig. 16, $P = 0.2$). Furthermore, *TIR1* silencing is partly mediated by Set1-dependent histone H3 lysine 4 methylation (H3K4me) because disrupting the Set1 catalytic activity re-established high levels of *TIR1* RNA as shown in *xrn1Δset1Δ*, *xrn1Δset1G951S* and *xrn1ΔH3K4A* strains (Fig. 4b, c and Supplementary Fig. 17a, b). To dissect the Set1 role, we compared the H3K4me1, H3K4me2 and H3K4me3 levels[28] in the wild type over the genes with antisense XUTs. Class 3 genes show H3K4me1/2/3 patterns (Fig. 4d) equivalent to all ORFs (Supplementary Fig. 18). By contrast, class 1 genes present 60% reduction of H3K4me3 levels but normal H3K4me2/me1 patterns (Fig. 4e). This indicates that although they have similar RNAPII distribution as class 3 genes (Supplementary Fig. 19), class 1 genes are marked and/or sensitized to their respective antisense ncRNA by low H3K4me3 levels. A tantalizing hypothesis is that antisense ncRNA-mediated gene silencing requires H3K4me1 and/or me2 but is antagonized by H3K4me3. Our model predicts that class 1 but also class 3 genes would be further silenced in absence of H3K4me3. To test this possibility, we performed analyses in a strain specifically depleted for H3K4me3 (H3R2Q mutant), without disrupting the Set1 complex[29]. In addition to a synergetic repression of *TY1* and *TIR1* mRNA (class 1 genes), we observed a decrease of the class 3 *LAC1* RNA levels in the *H3R2Qxrn1Δ* strain (Fig. 4f and Supplementary Fig. 20a). H3K4me3 is not involved in the expression of the respective antisense XUTs, similarly expressed in the *xrn1Δ* and *H3R2Qxrn1Δ* strains (Supplementary Fig. 20b). By contrast the *PGK1* and *YJU3* genes (class 4), both devoid of antisense XUTs, were not affected in *H3R2Qxrn1Δ*, supporting a model in which H3K4me3 antagonizes the negative activity of antisense ncRNA potentially associated with unknown silencing factors (Fig. 4g).

In conclusion, our results provide evidence for a novel class of cryptic antisense transcripts degraded by the cytoplasmic 5′–3′ RNA decay pathway. We propose that Set1-dependent histone methylation has a key role in controlling the antisense ncRNA-repressive activity using H3K4me3 as a molecular switch. Given the broad class of XUTs, we already anticipate also a post-transcriptional role(s). Because the key components of this pathway are distributed among the eukaryotic kingdom, the mechanism is likely to be conserved throughout evolution.

METHODS SUMMARY

RNA-seq libraries were generated according to the manufacturer's instructions using ribo$^-$/polyA$^+$ RNAs extracted from *S. cerevisiae* strains. ChIP-seq was performed according to Illumina protocols and sequenced on GAIIx. Tag profiles were analysed using appropriated biocomputational and statistical approaches (Methods). Northern-blot and ChIP (using anti-Rpb1-CTD 8wg16 antibody) were performed using standard techniques (Methods). Sequence data are publicly available at NCBI Sequence Read Archive under accession number SRA030505 and at http://vm-gb.curie.fr/XUT/index.htm.

Full Methods and any associated references are available in the online version of the paper at www.nature.com/nature.

Received 31 December 2010; accepted 14 April 2011.
Published online 22 June 2011.

1. Bernstein, E. & Allis, C. D. RNA meets chromatin. *Genes Dev.* **19,** 1635–1655 (2005).
2. Moazed, D. Small RNAs in transcriptional gene silencing and genome defence. *Nature* **457,** 413–420 (2009).
3. Swiezewski, S., Liu, F., Magusin, A. & Dean, C. Cold-induced silencing by long antisense transcripts of an *Arabidopsis* Polycomb target. *Nature* **462,** 799–802 (2009).
4. Yu, W. *et al.* Epigenetic silencing of tumour suppressor gene *p15* by its antisense RNA. *Nature* **451,** 202–206 (2008).
5. Yap, K. L. *et al.* Molecular interplay of the noncoding RNA *ANRIL* and methylated histone H3 lysine 27 by polycomb CBX7 in transcriptional silencing of *INK4a*. *Mol. Cell* **38,** 662–674 (2010).
6. Huarte, M. & Rinn, J. L. Large non-coding RNAs: missing links in cancer? *Hum. Mol. Genet.* **19,** R152–R161 (2010).
7. Chow, J. & Heard, E. X inactivation and the complexities of silencing a sex chromosome. *Curr. Opin. Cell Biol.* **21,** 359–366 (2009).
8. Nagano, T. *et al.* The *Air* noncoding RNA epigenetically silences transcription by targeting G9a to chromatin. *Science* **322,** 1717–1720 (2008).
9. Amaral, P. P., Dinger, M. E., Mercer, T. R. & Mattick, J. S. The eukaryotic genome as an RNA machine. *Science* **319,** 1787–1789 (2008).
10. Berretta, J. & Morillon, A. Pervasive transcription constitutes a new level of eukaryotic genome regulation. *EMBO Rep.* **10,** 973–982 (2009).
11. Camblong, J. *et al. Trans*-acting antisense RNAs mediate transcriptional gene cosuppression in *S. cerevisiae*. *Genes Dev.* **23,** 1534–1545 (2009).
12. Berretta, J., Pinskaya, M. & Morillon, A. A cryptic unstable transcript mediates transcriptional *trans*-silencing of the Ty1 retrotransposon in *S. cerevisiae*. *Genes Dev.* **22,** 615–626 (2008).
13. Matsuda, E. & Garfinkel, D. J. Posttranslational interference of Ty1 retrotransposition by antisense RNAs. *Proc. Natl Acad. Sci. USA* **106,** 15657–15662 (2009).
14. Aravind, L., Watanabe, H., Lipman, D. J. & Koonin, E. V. Lineage-specific loss and divergence of functionally linked genes in eukaryotes. *Proc. Natl Acad. Sci. USA* **97,** 11319–11324 (2000).
15. Jacquier, A. The complex eukaryotic transcriptome: unexpected pervasive transcription and novel small RNAs. *Nature Rev. Genet.* **10,** 833–844 (2009).
16. Long, R. M. & McNally, M. T. mRNA decay: X (*XRN1*) marks the spot. *Mol. Cell* **11,** 1126–1128 (2003).
17. Nagalakshmi, U. *et al.* The transcriptional landscape of the yeast genome defined by RNA sequencing. *Science* **320,** 1344–1349 (2008).
18. Neil, H. *et al.* Widespread bidirectional promoters are the major source of cryptic transcripts in yeast. *Nature* **457,** 1038–1042 (2009).
19. Yassour, M. *et al.* Strand-specific RNA sequencing reveals extensive regulated long antisense transcripts that are conserved across yeast species. *Genome Biol.* **11,** R87 (2010).
20. Chernyakov, I., Whipple, J. M., Kotelawala, L., Grayhack, E. J. & Phizicky, E. M. Degradation of several hypomodified mature tRNA species in *Saccharomyces cerevisiae* is mediated by Met22 and the 5′–3′ exonucleases Rat1 and Xrn1. *Genes Dev.* **22,** 1369–1380 (2008).
21. Fatica, A., Morlando, M. & Bozzoni, I. Yeast snoRNA accumulation relies on a cleavage-dependent/polyadenylation-independent 3′-processing apparatus. *EMBO J.* **19,** 6218–6229 (2000).
22. Xu, Z. *et al.* Bidirectional promoters generate pervasive transcription in yeast. *Nature* **457,** 1033–1037 (2009).
23. Thompson, D. M. & Parker, R. Cytoplasmic decay of intergenic transcripts in *Saccharomyces cerevisiae*. *Mol. Cell. Biol.* **27,** 92–101 (2007).
24. Wyers, F. *et al.* Cryptic pol II transcripts are degraded by a nuclear quality control pathway involving a new poly(A) polymerase. *Cell* **121,** 725–737 (2005).
25. Dichtl, B., Stevens, A. & Tollervey, D. Lithium toxicity in yeast is due to the inhibition of RNA processing enzymes. *EMBO J.* **16,** 7184–7195 (1997).
26. Johnson, A. W. Rat1p and Xrn1p are functionally interchangeable exoribonucleases that are restricted to and required in the nucleus and cytoplasm, respectively. *Mol. Cell. Biol.* **17,** 6122–6130 (1997).
27. Pinskaya, M. & Morillon, A. Histone H3 lysine 4 di-methylation: a novel mark for transcriptional fidelity? *Epigenetics* **4,** 302–306 (2009).
28. Pokholok, D. K. *et al.* Genome-wide map of nucleosome acetylation and methylation in yeast. *Cell* **122,** 517–527 (2005).
29. Kirmizis, A. *et al.* Arginine methylation at histone H3R2 controls deposition of H3K4 trimethylation. *Nature* **449,** 928–932 (2007).

Supplementary Information is linked to the online version of the paper at www.nature.com/nature.

Acknowledgements We thank B. Séraphin, L. Bénard and J. O'Sullivan for support and advice; B. Dichtl for insights into lithium treatment data normalization; M. Wéry and A. Taddei for helpful discussions; A. Johnson, T. Kouzarides and V. Géli for generous gift of plasmids and strains. Special thanks to M. Descrimes, C. Jubin and S. Lair for technical assistance. We thank L. Steinmetz and M. Chodder for sharing unpublished results. E.L.V.D. benefits from an FRM fellowship. This work has benefited from facilities and expertise of the IMAGIF sequencing platform (Centre de Recherche de Gif). This work was financially supported by the Canceropole Ile de France, the ANR "REGULncRNA" and ERC "EPIncRNA" starting grant.

Author Contributions E.L.V.D. performed molecular biology experiments, RNA-seq, ChIP-seq libraries and sequencing on the ILLUMINA platform. C.L.C., Y.D.-C., M.S. and C.T. performed statistical and bioinformatic analyses. S.G., M.K., V.R. and C.B. provided technical assistance to molecular biology experiments. A.M., C.T., E.L.V.D. and C.L.C. designed the experiments. P.L.-N. and S.L. performed RNA-seq libraries and NGS sequencing on the SOLiD platform; A.N. managed sequencing on the SOLiD platform. E.L.V.D., C.L.C. and A.N. contributed to the writing. C.T. and A.M. wrote the paper. C.T. and A.M. planned the project.

Author Information Sequence data are publicly available at NCBI Sequence Read Archive under accession number SRA030505 and at http://vm-gb.curie.fr/XUT/index.htm. Reprints and permissions information is available at www.nature.com/reprints. The authors declare no competing financial interests. Readers are welcome to comment on the online version of this article at www.nature.com/nature. Correspondence and requests for materials should be addressed to A.M. (antonin.morillon@curie.fr) or C.T. (thermes@cgm.cnrs-gif.fr).

METHODS

Yeast strains and growth media. Strains used in this study are from the Euroscarf collection (S288C, BY4741 background), except for the RNAPII and histone H3 studies. For RNAPII, we used the strains *rpb1-1* and *rpb1-1xrn1Δ* (ref. 12). For histone H3 we used strains WT-H3, *H3K4A*, *xrn1Δ* and *H3K4Axrn1Δ* previously manipulated[12] and WT-H3, *H3R2A* and *H3R2Q* generously provided by T. Kouzarides[29] in which we deleted *XRN1* gene (this work). The list of BY strains is WT, *xrn1Δ*, *set1Δ*, *set1Δxrn1Δ*, *trf4Δ*, *xrn1Δtrf4Δ*, *set1G951S* and *set1G951Sxrn1Δ*. The *set1G951S* strain was kindly provided by V. Géli. Gene deletions were introduced by transformation of PCR fragments generated with specific primers (sequences can be obtained upon request) using the appropriate plasmids[30].

Growth media were prepared by standards methods using rich YPDA media (yeast peptone dextrose adenine, Gibco) or minimal CSM media (MP biochemical) containing 2% glucose.

For lithium induction, cells were grown in CSM media and then transferred during the indicated time in CSM media with 100 mM lithium as indicated[25].

For Xrn1 conditional mutant experiments, the *xrn1Δ* strain was transformed with a wild-type *XRN1* plasmid (PAM27, pAJ52) or *xrn1ts* plasmid (PAM143, pAJ53), both plasmids from a gift from A. Johnson. Transformed cells were grown in CSM-URA media with glucose at 30 °C. Heat shock was performed at 37 °C and cells collected at the indicated times.

RNA extraction, polyA$^+$ and ribo$^-$ RNA purifications. Total RNA was extracted using the hot phenol extraction procedure. PolyA$^+$ RNAs were purified on oligodT Dynabeads (Invitrogen) and ribosomal RNA were depleted using the RiboMinus kit (Invitrogen). RNA quality was checked on agarose gel (Supplementary Fig. 2) and with the Bioanalyzer (Agilent) ensuring the quantification of RNA peaks recommended by the manufacturer.

Northern blotting. RNAs were loaded on denaturing 1% agarose gels containing formaldehyde and transferred to nitrocellulose membranes (Hybond XL). Membranes were cross-linked by ultraviolet irradiation and hybridized over-night at 65 °C with either ^{32}P-labelled DNA probes or oligonucleotide probes in PERFECT-HYB PLUS buffer (Sigma). Blots were washed at 65 °C for 10 min once with 2× SSC, 1% SDS and twice with 0.1× SSC, 1% SDS. DNA probes were obtained by random primed labelling (Stratagene) of specific DNA fragments generated by PCR. PCR primers are available upon request. *PGK1* and *scR1* RNAs were used as loading controls. Northern signals were quantified using ImageQuant software, normalized with *scR1* or *PGK1* intensities and wild-type ratios were set arbitrarily to 1. Error bars correspond to the standard deviation over three independent cultures.

Reverse transcription. Reverse transcription was performed according to the manufacturer's instructions (Invitrogen, SuperScript) on total RNA. Specific primers were used to amplify *TIR1axut*, *LAC1axut* and *scR1* loading control. Quantitative PCR were performed with the LightCycler 480 (Roche) using SYBR Green. PCR were normalized with *scR1* signals and wild-type ratios adjust to 1 for comparison. Error bars correspond to standard deviation over three independent reverse transcription reactions.

5′ RACE analysis. 5′ RACE experiments were done using a Firstchoice RLM-RACE kit from Ambion following the manufacturer's instructions. Total RNA from wild-type or *xrn1Δ* cells was used. Reverse transcription was performed with primers A, B, and C to detect the 5′ ends of *SUC2uxut* (Supplementary Fig. 7). Subsequently, PCR was done using nested primers (sequences available upon request). PCR products were cloned and sequenced.

Chromatin immunoprecipitation. Chromatin immunoprecipitations were performed essentially as described previously[12]. Yeast strains were grown to $D_{600} = 0.5$ in YPDA at 30 °C, and cross-linked 20 min by the addition of formaldehyde to a final concentration of 1.2%. Crosslinked reaction was quenched by adding glycine at 0.5 M final concentration. Chromatin was sonicated to obtain 400–500 nucleotides DNA fragment and 200 μg of sonicated chromatin was immunoprecipitated for 3 h at 21 °C on Pan mouse Dynabeads (Invitrogen) coated with specific antibody against the carboxy-terminal domain of Rpb1 (8WG16, Millipore). All immunoprecipitations were repeated at least three times with different chromatin extracts. Immunoprecipitated DNA was quantified by real-time PCR using the LightCycler 480 (Roche) with primer pairs (sequences available upon request). Signals are expressed as percentage of input DNA relatively to *RPO21* (coordinate: chromosome 4: 210562 to 205361). Error bars correspond to standard deviations of three independent experiments.

Library preparation for RNA-seq. The extracted RNAs (polyA$^+$ or ribo$^-$) were submitted to RNA fragmentation as recommended in the ABI whole transcriptome library preparation kit. RNA adaptors were ligated before cDNA preparation to ensure strand recognition. Typically, DNAs ranging from 150 to 250 nucleotides were size-selected on polyacrylamide gel followed by PCR amplification (15 cycles). Denatured single-stranded DNA was then hybridized on beads before emulsion PCR and deposited on SOLiD slides for sequencing. Runs were performed on the SOLiD V3 sequencing machine and 50 nucleotides single reads were generated on colour code format.

For Illumina sequencing, RNAs were subjected to sequencing on the Genome Analyzer IIx sequencing machine and 38 nucleotides reads were generated. The same polyA$^+$ samples as for the SOLiD libraries (but with Illumina adapters added by PCR) were used to confirm that sequencing technologies do not introduce bias in the reads. The duplicates libraries for wild type and *xrn1Δ*, lithium and *ts* were sequenced with Illumina technology (Supplementary Table 1).

Library preparation for ChIP-seq. For ChIP-seq, chromatin immunoprecipitation was done as described above, the only modification being that reactions were scaled up to obtain sufficient amounts of material for library preparation. Instead of 200 μg, 800 μg of sonicated chromatin was used. The sequences were obtained on Genome Analyzer IIx sequencer with 38 nucleotides reads (Supplementary Table 1).

Sequencing data. For SOLiD sequencing, 50-nucleotide sequence reads were identified using the standard SOLiD base-calling software and then aligned to the reference genome (*Saccharomyces cerevisiae* S288c retrieved from SGD, http://www.yeastgenome.org/) using Mapreads (v2.4.1) software allowing up to six mismatches. For Illumina/Solexa sequencing, 38-nucleotide sequence reads were identified using the standard Illumina base-calling software and then aligned to the reference genome using the ELAND (CASAVA pipeline) software allowing up to two mismatches within the 32-nucleotide seed. For multiplex samples, reads were partitioned and those lacking an intact barcode or index were discarded. Replicate experiments for ribo$^-$ samples produced read density values that strongly correlated to each other (Supplementary Fig. 4a, Pearson $R = 0.96$, $P < 10^{-15}$). Sequencing data obtained with the polyA$^+$/WT RNA sample using either the SOLiD or the Illumina/Solexa device were highly correlated to each other (Supplementary Fig. 4b, $R = 0.98$, $P < 10^{-15}$).

Transcriptome analysis and normalization. Genome was annotated according to SGD (http://www.yeastgenome.org/, 5 January 2010); SUT (stable unannotated transcript) and CUT (cryptic unstable transcript) annotations were retrieved[22]. Tag densities were computed for each transcript in each sample and in all cases, except for tRNAs, only tags mapping to unique positions were considered. Tag densities for tRNAs were computed (for each anticodon) by using the tags mapping to multiple positions. Except for the lithium and *set1Δ* transcriptomes, the tag densities were normalized in such a way that snoRNAs and tRNAs present the same levels in the wild-type and *xrn1Δ* strains (Supplementary Figure 3). The candidate transcripts obtained by the segmentation process that presented an *xrn1Δ*/WT ratio significantly larger than the background ratio were retained as XUTs. To determine whether the expression level of a gene (ORF) was significantly different in the *xrn1Δ* and wild-type strains, a *P*-value was computed based on negative binomial distribution (edgeR package[31] from Bioconductor, http://www.bioconductor.org/); for this comparison, individual ORF expression levels in the *xrn1Δ* and wild-type strains were compared to the ratio of the corresponding mean ORF expression values; transcripts with a *P*-value < 0.01 were retained. In the wild-type strain, a fraction of XUTs presents expression levels close to the background level of the density profile; to compare XUT expression levels in the ribo$^-$ and polyA$^+$ samples, only those presenting levels 50% higher than the background level of the corresponding profile were retained.

An extensive study was performed to identify the best way to normalize the RNA-seq values in the presence of lithium. As suggested by previous studies[25], tRNAs and snoRNAs levels are affected by lithium addition with mean ratios of 1.8 and 2.1, respectively (Supplementary Fig. 11a–d). In contrast, ribosomal proteins genes-derived transcripts present only a slight increase (1.5 fold) in the *xrn1Δ* strain, and are insensitive to lithium addition (mean ratio of 1.1, Supplementary Fig. 11e, f). The mean ribosomal proteins genes transcript value was thus used as reference to normalize RNA-seq values in the presence of lithium.

For the *set1Δ* transcriptome, levels were normalized by the mean level of all ORFs taken as reference, because the Set1 complex controls snoRNA transcription[32].

Segmentation of massive sequencing data. The RNA-seq procedure generates considerable variation of tag coverage along genes complicating the segmentation process. To address this problem, we designed a crude heuristic to detect candidate transcripts. Segmentation was performed on massive sequencing data obtained from the ribo$^-$ samples extracted from the *xrn1Δ* strain. The tag profile was built by computing the tag density within a sliding 120 base pairs (bp) window, using a 1-bp step size; segments were delimited on the tag profile using a threshold of 0.06 tag per nucleotide (50% of the annotated CUTs present a tag density lower than this threshold). To define transcripts, the extremities of each segment were adjusted to the first and last internal tags. Segments overlapping genes annotated on the same strand (ORFs, stable RNAs) were then removed. The remaining consecutive segments of similar densities (ratio smaller than twofold) distant by less than 250 bp were joined (only the 5′ end of the RNA pieces obtained by fragmentation of the initial transcripts was sequenced); the resulting segments longer than 250 bp were retained as final transcripts corresponding to 543

SUTs, 183 CUTs and 932 new transcripts (New). The extremities of XUTs tested experimentally were manually repositioned according to experimental data. With this procedure, previously defined SUTs were covered at 87% by the detected segments and the segments intersecting the SUTs were covered at 80% by the SUTs; in addition, 90% of the SUTs were covered by a unique detected segment (Supplementary Fig. **5**).

XUTs are polyadenylated and RNAPII dependent. Among the 1,658 XUTs, 683 were detected at low levels in the wild-type ribo$^-$ sample. Interestingly, 493 (72%) were also detected within the polyA$^+$ fraction (Supplementary Fig. 8a, b), strongly supporting that XUTs are polyadenylated, as shown for *PHO84*-, *GAL10*- and *TY1*-associated ncRNAs[12,33,34]. To confirm that XUTs are synthesized by RNAPII, we monitored the steady-state levels of the *SUC2uxut1* and *SUC2uxut3* mRNAs upon depletion of Rpb1, the main subunit of RNAPII (ref. 35). The *SUC2uxut1* mRNA levels were significantly reduced after 60 min of RNAPII inactivation similarly to the class 2 *ACT1* mRNA (Supplementary Fig. 8c, d). In contrast, the levels of *scR1* and rRNA, transcribed by RNA polymerase III and I, respectively, remained constant. Altogether these data support that XUTs RNA are polyadenylated and synthesized by the RNA polymerase II.

Analysis of *xrn1* conditional mutant. To examine possible late secondary effects of *XRN1* deletion, we asked whether a conditional mutant of Xrn1 would rapidly accumulate XUTs after Xrn1 inactivation and show repression of the same group of genes defined in Fig. 3a (class 1) . To answer this question, we determined the kinetics of the ncRNA-mediated Ty1 regulation using an *xrn1* thermosensitive (ts) mutant[26]. Interestingly, *TY1* ncRNA accumulated around 30 min after heat shock (Supplementary Figure 14a). In addition, *TY1* ncRNA accumulation preceded the decrease of the *TY1* mRNA starting approximately at 60 min, confirming the causal link between XUT accumulation and gene repression[12,13]. Interestingly, the *TY1* ncRNA kinetics reflect other XUTs dynamic because *SUC2uxut1*, *SUC2uxut3* and *TPO1axut* also appeared at 30 min, indicating a rapid and general accumulation of the XUTs upon Xrn1 inactivation. Indeed, RNA-seq experiments showed that 75% of the XUTs detected in *xrn1Δ* strain accumulated similarly after 90 min of Xrn1 inactivation (Supplementary Fig. 14b–d), indicating that XUTs are primary targets of Xrn1 RNA decay pathway. To determine whether the regulation of class 1 genes is a late or early event, we performed RNAPII-ChIP experiments in the *xrn1Δ* and *xrn1ts* strains (after 180 min in 37 °C) on a selection of genes belonging to the different classes defined in Figure 3a. Strikingly, the class 1 genes showed a similar decrease of RNAPII occupancy in the two *XRN1*-defective strains (Figure 3c), indicating that Xrn1 inactivation has an early effect on RNAPII on those genes. By contrast, the class 2 genes are only suppressed in *xrn1Δ* strain supporting a late and likely indirect effect of Xrn1 inactivation on those genes. We conclude that the class 1 genes are directly controlled by Xrn1, potentially though their respective antisense ncRNAs.

30. Longtine, M. S. *et al*. Additional modules for versatile and economical PCR-based gene deletion and modification in *Saccharomyces cerevisiae*. *Yeast* **14,** 953–961 (1998).
31. Robinson, M. D., McCarthy, D. J. & Smyth, G. K. edgeR: a Bioconductor package for differential expression analysis of digital gene expression. *Bioinformatics* **26,** 139–140 (2010).
32. Dichtl, B., Aasland, R. & Keller, W. Functions for *S. cerevisiae* Swd2p in 3′ end formation of specific mRNAs and snoRNAs and global histone 3 lysine 4 methylation. *RNA* **10,** 965–977 (2004).
33. Pinskaya, M., Gourvennec, S. & Morillon, A. H3 lysine 4 di- and tri-methylation deposited by cryptic transcription attenuates promoter activation. *EMBO J.* **28,** 1697–1707 (2009).
34. Camblong, J., Iglesias, N., Fickentscher, C., Dieppois, G. & Stutz, F. Antisense RNA stabilization induces transcriptional gene silencing via histone deacetylation in *S. cerevisiae*. *Cell* **131,** 706–717 (2007).
35. Nonet, M., Scafe, C., Sexton, J. & Young, R. Eucaryotic RNA polymerase conditional mutant that rapidly ceases mRNA synthesis. *Mol. Cell. Biol.* **7,** 1602–1611 (1987).